

Superconducting properties in a candidate topological nodal line semimetal SnTaS₂ with a centrosymmetric crystal structure

Dong-Yun Chen^{1,2,3}, Yuelong Wu¹, Lei Jin⁴, Yongkai Li^{2,3}, Xiaoxiong Wang¹, Junxi Duan^{2,3}, Junfeng Han^{2,3}, Xiang Li^{2,3}, Yun-Ze Long¹, Xiaoming Zhang⁴, Dong Chen^{1,*}, and Bing Teng^{1,†}

¹*College of Physics, Qingdao University, Qingdao 266071, China*

²*Key Laboratory of Advanced Optoelectronic Quantum Architecture and Measurement, Ministry of Education, School of Physics, Beijing Institute of Technology, 100081, Beijing*

³*Micronano Centre, Beijing Key Lab of Nanophotonics and Ultrafine Optoelectronic Systems, Beijing Institute of Technology, Beijing, 100081, China and*

⁴*School of Materials Science and Engineering, Hebei University of Technology, Tianjin 300130, China*

We report the magnetization, electrical resistivity, specific heat measurements and band structure calculations of layered superconductor SnTaS₂. The experiments are performed on single crystals grown by chemical vapor transport method. The resistivity and magnetic susceptibility indicate that SnTaS₂ is a type-II superconductor with transition temperature $T_c = 3$ K. The upper critical field (H_{c2}) shows large anisotropy for magnetic field parallel to ab plane ($H//ab$) and c axis ($H//c$), and the temperature dependence of H_{c2} for $H//ab$ shows obvious unconventional upward feature at low temperature. Band structure of SnTaS₂ shows several band crossings near the Fermi level, which form three nodal lines in the $k_z = 0$ plane resulting in drumhead-like surface states when spin-orbit coupling is not considered. These results indicate that SnTaS₂ is a superconductor with possible topological nodal line semimetal character.

INTRODUCTION

Superconductors with nontrivial band structure have attracted much attention due to the possibility of realizing some novel quantum states, such as topological superconductors and Majorana fermions [1, 2]. Nontrivial band structure has been found in both topological insulators and topological semimetals [1, 3–5]. Topological semimetals can be further classified according to the configuration of band crossing near the Fermi level, including Dirac semimetal, Weyl semimetal, nodal line semimetal, etc [6–11]. Superconductivity can be combined with the novel band structure by charge carrier doping or applying external pressure on topological materials. For example, topological insulator Bi₂Se₃ has been found superconducting when intercalated by Cu, Sr or Nb atoms [12–14], or subjected to high pressure [15]. Dirac semimetal Cd₃As₂ and type-II Weyl semimetal WTe₂ can be induced as superconductors under high pressure [16–18]. Besides, some topological materials themselves are superconductors. The type-II Weyl semimetal MoTe₂ has a superconducting transition with $T_c = 0.1$ K, and the T_c can be dramatically enhanced to 8.2 K with high pressure [19]. PbTaSe₂ is found as a superconducting topological nodal line semimetal with a noncentrosymmetric structure [20, 21]. The later category of aforementioned superconductors does not suffer topological state shift from charge carrier doping or high pressure, providing an excellent playground for researching superconductivity with nontrivial band topology.

The layered compound SnTaS₂, which is isoelectronic with PbTaSe₂, is another superconductor identified as early as 1973 [22]. Although the critical temperature for SnTaS₂ ($T_c = 2.8$ K) has been reported [22, 23],

more detailed superconducting properties are still unknown. Moreover, we notice that SnTaS₂ has a centrosymmetric structure, which is different from that of PbTaSe₂. Whether the centrosymmetric SnTaS₂ can host the topological nontrivial band structure is also unknown. In this paper, we have systemically investigated the superconducting properties and the electronic structure of SnTaS₂. The magnetization, electric transport, and specific heat properties are studied in detail on the single crystal samples. We find large anisotropy in the upper critical field and coherence length. The temperature dependence of the upper critical field has an obvious upward feature for magnetic field parallel to ab plane. Analysis of specific heat shows that SnTaS₂ is a moderately coupled superconductor. Using first principles calculations, we find that centrosymmetric SnTaS₂ exhibits a topological nodal line band structure when spin-orbit coupling (SOC) is not included. It features with three nodal lines centering the K point near the Fermi level, along with drumhead-like surface states corresponding to them. These properties are similar with those of PbTaSe₂. Our work suggests that SnTaS₂ is another system for investigating the novel properties of superconductors with topological nodal-line fermions.

EXPERIMENT AND METHODS

The single crystals of SnTaS₂ were grown by the chemical vapor transport method with iodine as the transport agent. Polycrystalline Sn_{0.33}TaS₂ was synthesized previously by the solid state reaction of Sn, Ta and S powders in an evacuated quartz tube at 850 °C. The obtained Sn_{0.33}TaS₂ polycrystals were mixed with Sn pow-

ders with element ratio Sn : Ta : S = 1.2 : 1 : 2 and sealed in an evacuated quartz tube together with iodine (3 mg/cm³ in concentration). The excess Sn was used to restrain the appearance of Sn_{0.33}TaS₂. The quartz tube was then put into a two-zone furnace with 1000 °C in hot zone and 970 °C in cold zone for two weeks. Thin plate shaped single crystals were obtained with typical dimensions of 3 × 3 × 0.05 mm³. The crystal structure of the obtained crystals was characterized by x-ray diffraction (XRD) on a Rigaku Smartlab x-ray diffractometer with Cu K α radiation at room temperature. The atomic ratio was determined by Oxford energy-dispersive x-ray (EDX) spectroscopy analysis. The magnetization, resistivity and specific heat of the samples were measured using a Quantum Design Physical Property Measurement System (PPMS).

The band structure calculations were performed based on the density functional theory (DFT), as implemented in the Vienna *ab initio* simulation package (VASP) [24]. The generalized gradient approximation (GGA) with the realization of Perdew-Burke-Ernzerhof (PBE) functional was adopted for the exchange-correlation potential [25]. The cutoff energy was set to be 450 eV and the Brillouin zone was sampled with a 13×13×5 Γ -centered k -mesh. The energy convergence criterion was chosen as 10⁻⁶ eV. The surface states were computed by using the Wannier_tools package [26].

RESULTS AND DISCUSSION

SnTaS₂ has a layered hexagonal structure (space group P6₃/mmc) with lattice parameters $a = b = 3.309$ Å, and $c = 17.450$ Å. The layered structure is formed by the alternative stacking of TaS₂ and Sn layers, as shown in Fig. 1(a). It should be noted that SnTaS₂ preserves the inversion and twofold screw rotation symmetries. Figure 1(b) is the XRD pattern of the maximum surface of a plate-like single crystal. All of the peaks can be indexed as the (00 l) reflections of SnTaS₂, indicating the single crystals perfectly oriented along the c -axis. The crystals can be further confirmed as SnTaS₂ by powder XRD and EDX measurements.

Figure 1(c) displays the typical temperature dependence of the resistivity for SnTaS₂ single crystals with current applied in the ab plane. The resistivity shows a metallic behavior and the residual resistivity ratio RRR = $\rho(300\text{ K})/\rho(4\text{ K})$ is as high as 380, indicating the high quality of the samples. The linear temperature dependence of the resistivity at high temperature suggests the dominance of electron-phonon scattering. As shown in the inset of Fig. 1(c), the resistivity has a sharp superconducting transition, and the critical temperature (T_c) can be determined as 3.0 K using the criterion of 50% point on the transition curve. To further demonstrate the superconductivity of the samples, we measured the

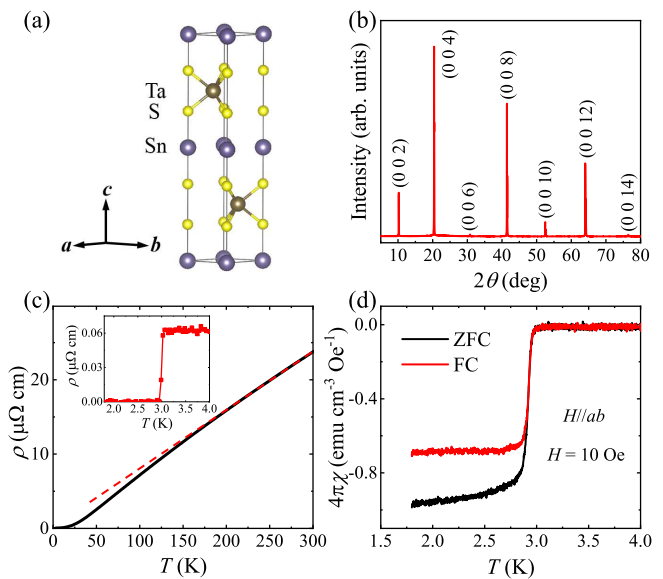


FIG. 1: (Color online)(a) Crystal structure of SnTaS₂. (b) The XRD pattern of SnTaS₂ single crystals with (00 l) reflections. (c) The temperature dependence of the resistivity with current flowing in the ab plane. The straight dashed line is the guide to the linear behaviour of the resistivity in high temperature. The inset shows the superconducting transition of resistivity. (d) The zero-field-cooling (ZFC) and field-cooling (FC) magnetic susceptibility curves measured with magnetic field of 10 Oe and parallel to the ab plane.

dc susceptibility in the zero-field-cooling (ZFC) and field-cooling (FC) processes with magnetic field of 10 Oe parallel to the ab plane, as displayed in Fig. 1(d). The demagnetization effect is not considered due to the thin plate shaped sample with magnetic field parallel to the sample plane. The T_c determined from the susceptibility curve is about 2.97 K, close to that determined from resistivity data. The superconducting shielding volume fraction at 1.8 K is close to 100%. In addition, the FC curve is not coincident with the ZFC curve, suggesting a type-II superconductor. However, the FC curve is not much larger than the ZFC curve, indicating few vortices pinning.

To estimate the anisotropic lower critical field (H_{c1}), the zero-field cooled magnetization $M(H)$ curves were measured with $H//ab$ and $H//c$, as shown in Fig. 2(a) and 2(c), respectively. The values of H_{c1} are determined as the points for $M(H)$ deviating 5% from the linear fitted curves. To get the accurate values of H_{c1} , the demagnetization effect should be considered. For a perfectly diamagnetic superconductor, the magnetic field lines are excluded from the inside of the sample and have higher density in the outside. This makes a higher field that the sample feels around it and a more pronounced diamagnetization slope, i. e. $M/H_a = -1/(1 - N)$, where N is the demagnetization factor. For the thin plate shaped sample, N is almost 0 for magnetic field parallel to the

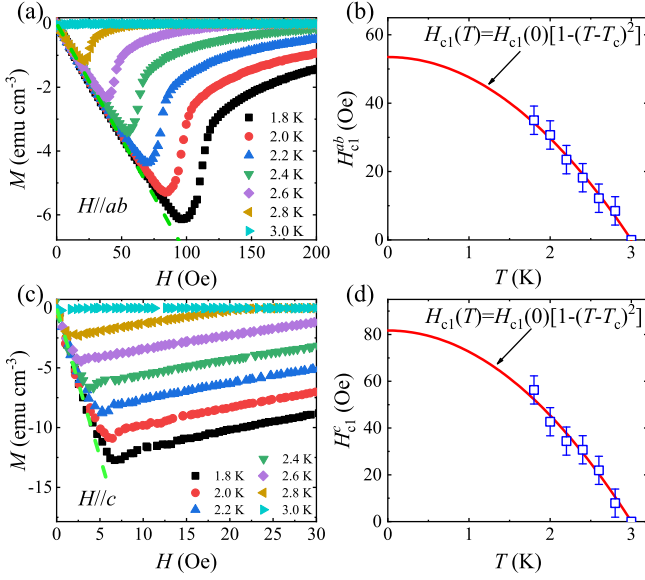


FIG. 2: (Color online) (a) (c) The zero-field cooled magnetization $M(H)$ curves at different temperatures with magnetic field parallel to the ab plane and c axis, respectively. The straight dashed lines are the linear fits to the 2 K curves in low-field range. (b) (d) The lower critical field for magnetic field parallel to the ab plane and c axis, respectively, with the fit lines using equation $H_{c1}(T) = H_{c1}(0)[1 - (T/T_c)^2]$. The demagnetization correction is considered in H_{c1}^c .

sample's surface and nearly 1 when magnetic field is perpendicular to the surface. Thus, for the thin SnTaS₂ plates, the H_{c1} for $H//ab$ (H_{c1}^{ab}) can be determined directly from the magnetization curves without demagnetization correction, as shown in Fig. 2(b). By contrast, the demagnetization correction can not be neglected when we determine the H_{c1} for $H//c$ (H_{c1}^c). To calculate the demagnetization factor N , we employ the relation [27]

$$N = 1 - 1 / \left(1 + q_{disk} \frac{a}{c} \right), \quad (1)$$

$$q_{disk} = \frac{4}{3\pi} + \frac{2}{3\pi} \tanh \left[1.27 \frac{c}{a} \ln \left(1 + \frac{a}{c} \right) \right], \quad (2)$$

where a and c are the dimension perpendicular to the magnetic field and the thickness of the sample, respectively. Here, the demagnetization correction has been considered in determining the values of H_{c1}^c in Fig. 2(d) with $N \approx 0.9473$. Both of the H_{c1}^c and H_{c1}^{ab} data can be fitted using $H_{c1}(T) = H_{c1}(0)[1 - (T/T_c)^2]$. The lower critical fields at zero temperature for the two directions are $H_{c1}^{ab}(0) = 53.5$ Oe and $H_{c1}^c(0) = 81.7$ Oe, respectively.

The low temperature resistivity under various magnetic fields with $H//c$ and $H//ab$ are presented in Fig. 3(a) and 3(c), respectively. The superconducting transition is very sharp for the zero-field curve and is broadened lightly by the applied fields. With the 50% criterion to determine the transition temperatures, the upper critical

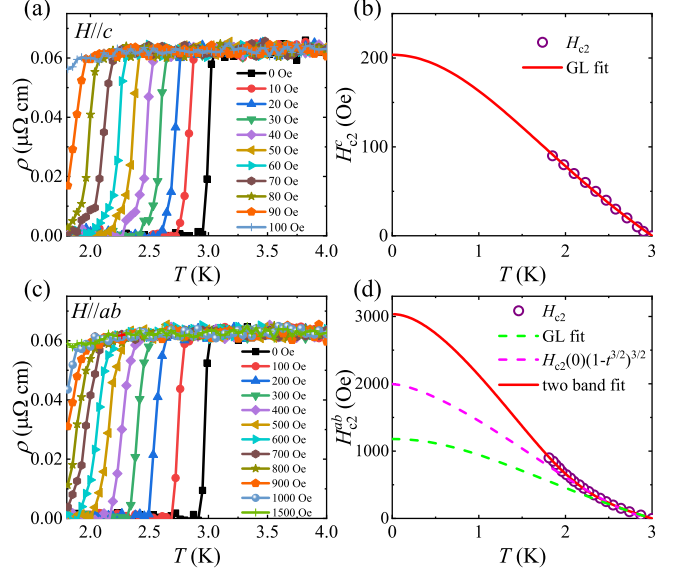


FIG. 3: (Color online) (a) (c) The low temperature $\rho(T)$ curves under different magnetic fields for $H//c$ and $H//ab$, respectively. (b) The temperature dependence of the upper critical field extracted from the resistivity curves with $H//c$. The data are fitted by GL equation. (d) The temperature dependence of the upper critical field extracted from the resistivity curves with $H//ab$. The data are fitted by three different equations.

fields for $H//c$ (H_{c2}^c) and $H//ab$ (H_{c2}^{ab}) as the functions of temperature are given in Fig. 3(b) and 3(d), respectively. The temperature dependence of H_{c2}^c can be well fitted with Ginzberg-Landau (GL) equation $H_{c2}(T) = H_{c2}(0)(1 - t^2)/(1 + t^2)$, where $t = T/T_c$. The upper critical field at $T = 0$ K for $H//c$ is accordingly estimated as $H_{c2}^c(0) = 203.6$ Oe. For $H//ab$, the temperature dependence of H_{c2}^{ab} has an obvious upward feature and deviates from the GL equation for $T < 2.5$ K. This upward feature for $H_{c2}^{ab}(T)$ is also found in PbTaSe₂ [20, 28–30], where the upper critical field can be roughly fitted by equation $H_{c2}(T) = H_{c2}(0)(1 - t^{3/2})^{3/2}$. However, the fitting curve using this formula is also lower than the $H_{c2}^{ab}(T)$ data in low temperature region (Fig. 3(d)), indicating the upward feature in SnTaS₂ is more obvious than that of PbTaSe₂.

The enhancement of H_{c2} in low temperature has several possible origins, such as: (1) dimensional crossover [31], (2) presence of impurities and disorder [32, 33], (3) multiband effect [34], (4) melting of the vortex lattice associate with quantum critical point [35], and (5) the non-local effect in the clean limit [36]. The dimensional crossover means that the superconductor changes from bulk superconductor to a stacked array of two-dimensional superconducting layers with the coherence length perpendicular to the layers (ξ_c) getting smaller than the distance between adjacent layers with decreasing temperature. This theory has been used to explain

TABLE I: The superconducting parameters of SnTaS₂ single crystal.

	$H//ab$	$H//c$
$H_{c1}(0)$ (Oe)	53.5	81.7
$H_{c2}(0)$ (Oe)	3034	203.6
$\xi(0)$ (nm)	127	8.5
$\kappa(0)$	7.58	5.07
$\lambda(0)$ (nm)	64.4	962.4
$\gamma_{\text{anis}}(0)$		14.9
$\Delta C/\gamma T_c$		1.23
Θ_D (K)		154.4
λ_{ep}		0.66

the upward curvature in $H_{c2}^{ab}(T)$ of organic molecules intercalated 2H-TaS₂ [37, 38], in which the H_{c2}^{ab} s can exceed the Pauli paramagnetic limit at moderate temperatures and the coherence lengths are comparable with the TaS₂ layer distance. In our case, the H_{c2}^{ab} is much smaller than the Pauli paramagnetic limiting field ($\mu_0 H_P = 5.5$ T) down to 1.8 K, and the ξ_c is much larger than the layer distance (see below). These facts demonstrate that the layers in SnTaS₂ are not decoupled and it is a bulk superconductor. On the other hand, the high value of RRR = 380 indicates the high quality and low density of defects in our samples. This excludes the possibility of the scattering by impurities and supports the non-local effect scenario. The current properties of SnTaS₂ show no trace for the quantum critical point. The result of DFT computations discussed later shows several bands cross the Fermi level. Therefore, the multiband effect and the non-local effect are the most likely origins for the upward curvature of $H_{c2}^{ab}(T)$.

To estimate $H_{c2}^{ab}(0)$, we try to fit the $H_{c2}^{ab}(T)$ data using the equation for a two-band superconductor [34], i. e.

$$a_0[\ln t + U(t)][\ln t + U(\eta h)] + a_1[\ln t + U(h)] + a_2[\ln t + U(\eta h)] = 0, \quad (3)$$

where $t = T/T_c$, $h = \frac{H_{c2} D_1}{2\phi_0 T}$, $\eta = \frac{D_2}{D_1}$, $U(x) = \psi(x + \frac{1}{2}) - \psi(\frac{1}{2})$, $a_0 = 2(\lambda_{11}\lambda_{22} - \lambda_{12}\lambda_{21})/\lambda_0$, $a_1 = 1 + (\lambda_{11} - \lambda_{22})/\lambda_0$, $a_2 = 1 - (\lambda_{11} - \lambda_{22})/\lambda_0$, and $\lambda_0 = \sqrt{(\lambda_{11} - \lambda_{22})^2 + 4\lambda_{12}\lambda_{21}}$. $\psi(x)$ is the digamma function. D_1 and D_2 are the intraband diffusivities of each band. λ_{11} and λ_{22} are the intraband coupling constants, whereas λ_{12} and λ_{21} are the interband coupling constants. As shown in Fig. 3(d), the experimental data can be well fitted by the two-band formula, which gives $H_{c2}^{ab}(0) = 3034$ Oe. The $H_{c2}^{ab}(0)$ is much lower than the Pauli limiting field, suggesting the upper critical field is limited by the orbital effect. The anisotropic ratio of H_{c2} , $\gamma_{\text{anis}}(0) = H_{c2}^{ab}(0)/H_{c2}^c(0)$, is as large as 14.9, larger than those of 2H-TaS₂ ($\gamma_{\text{anis}} = 6$) and PbTaSe₂ ($\gamma_{\text{anis}} = 11.6$) [29, 38].

Based on the GL theory, the anisotropic coherence

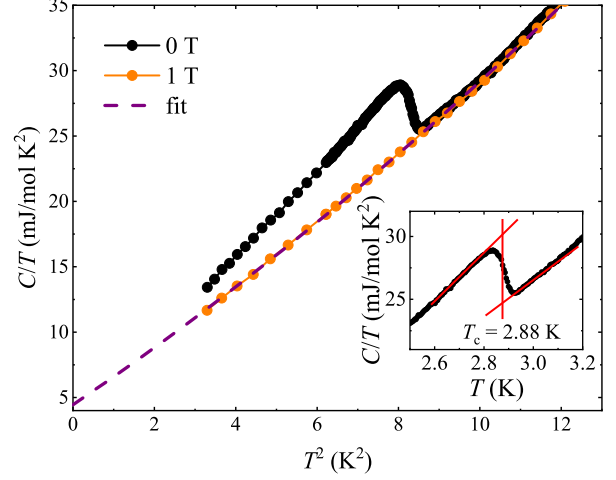


FIG. 4: (Color online) The specific heat divided by temperature (C/T) as the function of T^2 with $\mu_0 H = 0$ and 1 T. The curve for $\mu_0 H = 1$ T is fitted by relation $C/T = \gamma + \beta T^2 + \delta T^4$. The inset shows the isoentropic method for T_c determination.

length is given by $H_{c2}^{ab} = \Phi_0/(2\pi\xi_{ab}\xi_c)$ and $H_{c2}^c = \Phi_0/(2\pi\xi_{ab}^2)$, where Φ_0 is the flux quantum [39]. Accordingly, the anisotropic GL coherence length at zero temperature can be determined as $\xi_{ab}(0) = 127$ nm and $\xi_c(0) = 8.5$ nm, and the anisotropic ratio is $\xi_{ab}/\xi_c = 14.9$. As mentioned above, the ξ_c is much larger than the TaS₂ layer distance (~ 8.7 Å), indicating the bulk superconductivity of this system. The GL parameter $\kappa_i(0)$ along the i direction can be obtained by the equation $H_{c2}^i(0)/H_{c1}^i(0) = 2\kappa_i^2(0)/\ln\kappa_i(0)$. The GL parameter $\kappa_i(0)$ is related with the anisotropic GL penetration length $\lambda_i(0)$ and coherence length $\xi_i(0)$ by equations $\kappa_c(0) = \lambda_{ab}(0)/\xi_{ab}(0)$ and $\kappa_{ab}(0) = \lambda_{ab}(0)/\xi_c(0) = [\lambda_{ab}(0)\lambda_c(0)/\xi_{ab}(0)\xi_c(0)]^{1/2}$, in which $\xi_{ab}/\xi_c = \lambda_c/\lambda_{ab}$. With these relations, the GL parameter $\kappa_i(0)$ and the anisotropic $\lambda_i(0)$ can be determined, as listed in Table I.

To further investigate the superconducting properties of SnTaS₂, we performed specific heat measurements and analysis. The low temperature specific heat under the fields of $\mu_0 H = 0$ and 1 T are demonstrated as the relationships of C/T versus T^2 in Fig. 4. With $\mu_0 H = 0$ T, the specific heat shows a sharp jump at $T_c = 2.88$ K, which is determined by the isoentropic method shown in the inset. The superconducting transition is completely suppressed by magnetic field of 1 T, and the $C/T - T^2$ curve under $\mu_0 H = 1$ T can be well fitted by the formula $C/T = \gamma + \beta T^2 + \delta T^4$. The fit yields the normal state Sommerfeld coefficient $\gamma = 4.45$ mJ/mol K², and the phonon specific coefficient $\beta = 2.11$ mJ/mol K⁴. The value of $\Delta C/\gamma T_c$ is estimated as 1.23, which is smaller than the value of BCS theory (1.43). With the formula $\Theta_D = [(12/5\beta)\pi^4 n N_A k_B]^{1/3}$, where $n = 4$ for SnTaS₂ and N_A is the Avogadro constant, the Debye tempera-

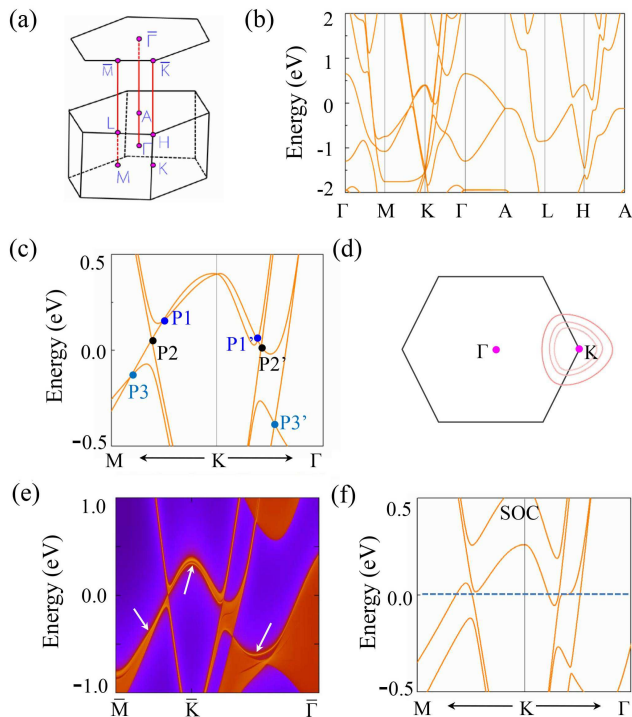


FIG. 5: (Color online) (a) Bulk and (001)-surface Brillouin zone of SnTaS₂. (b) Electronic band structure of SnTaS₂ without SOC. (c) Enlarged band structure along M-K and K- Γ paths. (d) Illustration of the three nodal lines centering the K point in the $k_z = 0$ plane. (e) The Sn-terminated (001) surface band structure for SnTaS₂. The drumhead-like surface states are pointed by white arrows. (f) Electronic band structure of SnTaS₂ with SOC included.

ture is estimated as $\Theta_D = 154.4$ K. The electron-phonon coupling constant λ_{ep} can be calculated using the McMillans Formula [40]:

$$\lambda_{ep} = \frac{1.04 + \mu^* \ln(\Theta_D/1.45T_c)}{(1 - 0.62\mu^*) \ln(\Theta_D/1.45T_c) - 1.04}. \quad (4)$$

The value of λ_{ep} is 0.66 assuming $\mu^* = 0.13$. This value is smaller than 1.0, the minimum value of strong coupling, indicating SnTaS₂ a moderately coupled superconductor. Both of the values of Θ_D and λ_{ep} are close to those of PbTaSe₂ [20, 28, 29]. With these results, the noninteracting density of states at Fermi level can be calculated by $N(E_F) = 3\gamma/[\pi^2 k_B^2 (1 + \lambda_{ep})]$, which gives $N(E_F) = 1.14$ states eV⁻¹ per formula unit. It can be noticed that the above parameters are different from those in the previous work [23]. This discrepancy may be due to the different sample quality caused by the changed growth conditions.

In view of the similarity in element component of SnTaS₂ with the topological nodal line semimetal PbTaSe₂, we study the band structure of SnTaS₂ through the first principles calculations. Figure 5(a) is the schematic diagram for bulk and (001)-surface Brillouin zone of SnTaS₂. Figure 5(b) clearly manifests a metal-

lic band structure with several bands crossing the Fermi level. As shown by the enlarged band structure in Fig. 5(c), there exist six band crossing points at M-K and K- Γ paths near the Fermi level without SOC in account. By performing more careful calculations on the band structure nearby, we find these band crossing points are not isolated but belong to three nodal lines centering the K point in the $k_z = 0$ plane, as shown in Fig. 5(d). This indicates SnTaS₂ is a topological nodal line semimetal in the absence of SOC. In addition, the drumhead-like surface states from the nodal lines are quite visible, as pointed by the arrows in Fig. 5(e). When SOC is included, the nodal lines in SnTaS₂ are gapped, as shown in Fig. 5(f). The sizes of SOC gaps in SnTaS₂ are in the range of 15-180 meV, which are comparable with typical nodal line materials such as TiB₂, Cu₃PdN, Mg₃Bi₂, and CaAgAs [41–45]. From Fig. 5(b) and (f), we can observe several electron-like and hole-like bands cross the Fermi level, consistent with the multiband scenario which is a possible origin for the upward curvature of $H_{c2}^{ab}(T)$ in our samples. The density of states at Fermi level calculated from the band structure is 1.04 states eV⁻¹ per formula unit with SOC, in good agreement with the value obtained from specific heat measurements.

It is interesting that, similar with PbTaSe₂, SnTaS₂ is also a superconducting nodal line semimetal, which is isoelectronic but not isostructural with PbTaSe₂. Although they have the similar electronic structure, the nodal lines in these two materials come from different origins. The nodal lines in noncentrosymmetric PbTaSe₂ are protected by the mirror reflection symmetry [21], while the nodal lines in SnTaS₂ are protected by time-reversal and inversion symmetries. The different symmetries cause that, when SOC is considered, the nodal lines are persistent in PbTaSe₂ but gapped in SnTaS₂ [21]. These common and different properties with PbTaSe₂ make SnTaS₂ as a great platform to further investigate the properties of superconducting nodal line semimetals.

CONCLUSION

In summary, we report the magnetic, transport, specific heat properties and electronic structure of centrosymmetric compound SnTaS₂, which is a layered type-II superconductor. Large anisotropy is found in the upper critical field and GL coherence length. An obvious upward curvature is observed in the upper critical field curve for $H//ab$, maybe due to the multiband effect or the non-local effect, which needs further investigations to clarify. The electron-phonon coupling constant is determined as 0.66, indicating a moderately coupled superconductor. The band structure of SnTaS₂ exhibits three nodal lines in the $k_z = 0$ plane near the Fermi level with drumhead-like surface states. With the similar crystal structure but different symmetries with noncentrosym-

metric PbTaSe_2 , SnTaS_2 is considered as a promising system to research the novel properties of superconducting topological nodal line semimetals.

ACKNOWLEDGEMENTS

This work was supported by the National Natural Science Foundation of China (Grant No. 11804176, 11734003), the National Key Research and Development Program of China (Grant No. 2016YFA0300604), Shandong Provincial Natural Science Foundation, China (Grant No. ZR2018BA030), and China Postdoctoral Science Foundation (Grant No. 2018M632609).

*dchen@qdu.edu.cn

†5108tb@163.com

-
- [1] X.-L. Qi and S.-C. Zhang, *Rev. Mod. Phys.* **83**, 1057 (2011).
- [2] L. Fu and C. L. Kane, *Phys. Rev. Lett.* **100**, 096407 (2008).
- [3] M. Z. Hasan and C. L. Kane, *Rev. Mod. Phys.* **82**, 3045 (2010).
- [4] H. Zhang, C.-X. Liu, X.-L. Qi, X. Dai, Z. Fang, and S.-C. Zhang, *Nat. Phys.* **5**, 438 (2009).
- [5] N. P. Armitage, E. J. Mele, and A. Vishwanath, *Rev. Mod. Phys.* **90**, 015001 (2018).
- [6] Z. Wang, Y. Sun, X.-Q. Chen, C. Franchini, G. Xu, H. Weng, X. Dai, and Z. Fang, *Phys. Rev. B* **85**, 195320 (2012).
- [7] H. Weng, C. Fang, Z. Fang, B. A. Bernevig, and X. Dai, *Phys. Rev. X* **5**, 011029 (2015).
- [8] A. A. Soluyanov, D. Gresch, Z. Wang, Q. Wu, M. Troyer, X. Dai, and B. A. Bernevig, *Nature* **527**, 495 (2015).
- [9] L. M. Schoop, M. N. Ali, C. Straer, A. Topp, A. Varykhalov, D. Marchenko, V. Duppel, S. S. P. Parkin, B. V. Lotsch, and C. R. Ast, *Nat. Commun.* **7**, 11696 (2016).
- [10] X. Zhang, Z.-M. Yu, Z. Zhu, W. Wu, S.-S. Wang, X.-L. Sheng, and S. A. Yang, *Phys. Rev. B* **97**, 235150 (2018).
- [11] H. Weng, C. Fang, Z. Fang, and X. Dai, *Phys. Rev. B* **93**, 241202(R) (2016).
- [12] Y. S. Hor, A. J. Williams, J. G. Checkelsky, P. Roushan, J. Seo, Q. Xu, H. W. Zandbergen, A. Yazdani, N. P. Ong, and R. J. Cava, *Phys. Rev. Lett.* **104**, 057001 (2010).
- [13] Z. Liu, X. Yao, J. Shao, M. Zuo, L. Pi, S. Tan, C. Zhang, and Y. Zhang, *J. Am. Chem. Soc.* **137**, 10512 (2015).
- [14] Y. Qiu, K. N. Sanders, J. Dai, J. E. Medvedeva, W. Wu, P. Ghaemi, T. Vojta, and Y. S. Hor, *arXiv preprint arXiv:1512.03519* (2015).
- [15] K. Kirshenbaum, P. S. Syers, A. P. Hope, N. P. Butch, J. R. Jeffries, S. T. Weir, J. J. Hamlin, M. B. Maple, Y. K. Vohra, and J. Paglione, *Phys. Rev. Lett.* **111**, 087001 (2013).
- [16] L. He, Y. Jia, S. Zhang, X. Hong, C. Jin, and S. Li, *npj Quant. Mater.* **1**, 16014 (2016).
- [17] D. Kang, Y. Zhou, W. Yi, C. Yang, J. Guo, Y. Shi, S. Zhang, Z. Wang, C. Zhang, S. Jiang, et al., *Nat. Commun.* **6**, 7804 (2015).
- [18] X.-C. Pan, X. Chen, H. Liu, Y. Feng, Z. Wei, Y. Zhou, Z. Chi, L. Pi, F. Yen, F. Song, et al., *Nat. Commun.* **6**, 7805 (2015).
- [19] Y. Qi, P. G. Naumov, M. N. Ali, C. R. Rajamathi, W. Schnelle, O. Barkalov, M. Hanfland, S.-C. Wu, C. Shekhar, Y. Sun, et al., *Nat. Commun.* **7**, 11038 (2016).
- [20] M. N. Ali, Q. D. Gibson, T. Klimczuk, and R. J. Cava, *Phys. Rev. B* **89**, 020505(R) (2014).
- [21] G. Bian, T.-R. Chang, R. Sankar, S.-Y. Xu, H. Zheng, T. Neupert, C.-K. Chiu, S.-M. Huang, G. Chang, I. Belopolski, et al., *Nat. Commun.* **7**, 10556 (2016).
- [22] F. J. Di Salvo, G. W. Hull Jr., L. H. Schwartz, J. M. Voorhoeve, and J. V. Waszczak, *J. Chem. Phys.* **59**, 1922 (1973).
- [23] J. Dijkstra, E. A. Broekhuizen, C. F. van Bruggen, C. Haas, R. A. de Groot, and H. P. van der Meulen, *Phys. Rev. B* **40**, 12111 (1989).
- [24] G. Kresse and D. Joubert, *Phys. Rev. B* **59**, 1758 (1999).
- [25] J. P. Perdew, K. Burke, and M. Ernzerhof, *Phys. Rev. Lett.* **77**, 3865 (1996).
- [26] Q. Wu, S. Zhang, H.-F. Song, M. Troyer, and A. A. Soluyanov, *Comput. Phys. Commun.* **224**, 405 (2018).
- [27] E. H. Brandt, *Phys. Rev. B* **60**, 11939 (1999).
- [28] C.-L. Zhang, Z. Yuan, G. Bian, S.-Y. Xu, X. Zhang, M. Z. Hasan, and S. Jia, *Phys. Rev. B* **93**, 054520 (2016).
- [29] Y.-J. Long, L.-X. Zhao, P.-P. Wang, H.-X. Yang, J.-Q. Li, H. Zi, Z.-A. Ren, C. Ren, and G.-F. Chen, *Chin. Phys. Lett.* **33**, 037401 (2016).
- [30] J. Wang, X. Xu, N. Zhou, L. Li, X. Cao, J. Yang, Y. Li, C. Cao, J. Dai, J. Zhang, et al., *J. Supercond. Nov. Magn.* **28**, 3173 (2015).
- [31] R. A. Klemm, A. Luther, and M. R. Beasley, *Phys. Rev. B* **12**, 877 (1975).
- [32] Y. N. Ovchinnikov and V. Z. Kresin, *Phys. Rev. B* **52**, 3075 (1995).
- [33] S. Maekawa, H. Ebisawa, and H. Fukuyama, *J. Phys. Soc. Jpn.* **52**, 1352 (1983).
- [34] A. Gurevich, *Phys. Rev. B* **67**, 184515 (2003).
- [35] G. Kotliar and C. M. Varma, *Phys. Rev. Lett.* **77**, 2296 (1996).
- [36] P. C. Hohenberg and N. R. Werthamer, *Phys. Rev.* **153**, 493 (1967).
- [37] D. E. Prober, R. E. Schwall, and M. R. Beasley, *Phys. Rev. B* **21**, 2717 (1980).
- [38] R. V. Coleman, G. K. Eiserman, S. J. Hillenius, A. T. Mitchell, and J. L. Vicent, *Phys. Rev. B* **27**, 125 (1983).
- [39] J. R. Clem, *Physica C* **162**, 1137 (1989).
- [40] W. L. McMillan, *Phys. Rev.* **167**, 331 (1968).
- [41] X. Zhang, Z.-M. Yu, X.-L. Sheng, H. Y. Yang, and S. A. Yang, *Phys. Rev. B* **95**, 235116 (2017).
- [42] Y. Kim, B. J. Wieder, C. L. Kane, and A. M. Rappe, *Phys. Rev. Lett.* **115**, 036806 (2015).
- [43] R. Yu, H. Weng, Z. Fang, X. Dai, and X. Hu, *Phys. Rev. Lett.* **115**, 036807 (2015).
- [44] X. Zhang, L. Jin, X. Dai, and G. Liu, *J. Phys. Chem. Lett.* **8**, 4814 (2017).
- [45] A. Yamakage, Y. Yamakawa, Y. Tanaka, and Y. Okamoto, *J. Phys. Soc. Jpn.* **85**, 013708 (2016).